

University of Groningen

Spintronics via non-axisymmetric chiral skyrmions

Leonov, A. O.; Loudon, J. C.; Bogdanov, A. N.

Published in:
 Applied Physics Letters

DOI:
[10.1063/1.4965981](https://doi.org/10.1063/1.4965981)

IMPORTANT NOTE: You are advised to consult the publisher's version (publisher's PDF) if you wish to cite from it. Please check the document version below.

Document Version
 Publisher's PDF, also known as Version of record

Publication date:
 2016

[Link to publication in University of Groningen/UMCG research database](#)

Citation for published version (APA):

Leonov, A. O., Loudon, J. C., & Bogdanov, A. N. (2016). Spintronics via non-axisymmetric chiral skyrmions. *Applied Physics Letters*, 109(17), [172404]. <https://doi.org/10.1063/1.4965981>

Copyright

Other than for strictly personal use, it is not permitted to download or to forward/distribute the text or part of it without the consent of the author(s) and/or copyright holder(s), unless the work is under an open content license (like Creative Commons).

The publication may also be distributed here under the terms of Article 25fa of the Dutch Copyright Act, indicated by the "Taverne" license. More information can be found on the University of Groningen website: <https://www.rug.nl/library/open-access/self-archiving-pure/taverne-amendment>.

Take-down policy

If you believe that this document breaches copyright please contact us providing details, and we will remove access to the work immediately and investigate your claim.

Downloaded from the University of Groningen/UMCG research database (Pure): <http://www.rug.nl/research/portal>. For technical reasons the number of authors shown on this cover page is limited to 10 maximum.

Spintronics via non-axisymmetric chiral skyrmions

A. O. Leonov,^{1,2,3,a)} J. C. Loudon,⁴ and A. N. Bogdanov^{1,2}

¹Center for Chiral Science, Hiroshima University, Higashi-Hiroshima, Hiroshima 739-8526, Japan

²IFW Dresden, Postfach 270016, D-01171 Dresden, Germany

³Zernike Institute for Advanced Materials, University of Groningen, Groningen 9700AB, The Netherlands

⁴Department of Materials Science and Metallurgy, 27 Charles Babbage Road, Cambridge CB3 0FS, United Kingdom

(Received 5 September 2016; accepted 11 October 2016; published online 28 October 2016)

Micromagnetic calculations demonstrate a peculiar evolution of non-axisymmetric skyrmions driven by an applied magnetic field in confined helimagnets with longitudinal modulations. We argue that these specific solitonic states can be employed in nanoelectronic devices as an effective alternative to the common axisymmetric skyrmions that occur in magnetically saturated states.

Published by AIP Publishing. [<http://dx.doi.org/10.1063/1.4965981>]

Two-dimensional topological solitons with an axisymmetric structure (commonly addressed as isolated *chiral skyrmions*¹) are stabilized by Dzyaloshinskii-Moriya (DM) interactions in the *saturated* states of noncentrosymmetric magnetic materials.² In magnetic nanolayers, chiral skyrmions represent nanosized spots of reverse magnetization that can be created or deleted by a magnetic tip³ and moved by electric currents and applied magnetic fields.^{1,3,4} Due to their remarkable properties, the magnetic skyrmions are considered promising objects for the next-generation memory and logic devices,^{5–7} which store information in the form of skyrmions that can be manipulated at room temperature.^{8–10}

In practice, isolated magnetic skyrmions are induced and manipulated in laterally confined saturated helimagnets (slabs, narrow strips, nanowires, and nanodots).^{1,3,7,11,12} Importantly, magnetic saturation is never fully reached in confined nanosystems as surface modulations occur near the sample edges (so called *chiral surface twists*)¹³ with a *penetration depth* estimated as $0.1p$ (p is the helix period at zero field).¹⁴ In the case of a narrow strip, the edge states manifest themselves as remnants of the helical spiral^{14–16} with a smooth deviation of the magnetization from being co-aligned with the field in the middle of the sample (Figs. 1(a) and 1(b)) to composing some (field- and anisotropy-dependent) angle θ_0 at the edge. To date, theoretical investigations of confined chiral skyrmions and their applications have been restricted to saturated helimagnets (Fig. 1(b)).^{6,17} In that case, the skyrmion-edge interaction has a repulsive character (Eq. (21) in Ref. 14) due to the same rotational sense of the magnetization in the *axisymmetric* skyrmions and the surface modulations.

In this paper, we address a special type of *non-axisymmetric* skyrmion introduced in Ref. 18. These three-dimensional solitonic states arise in the longitudinally modulated chiral ferromagnets (with the conical phase, Fig. 1(c)) and hence are inhomogeneous along their axes. Within the micromagnetic model, we calculate the structure of non-axisymmetric skyrmions and edge modulations in a confined chiral helimagnet. We show that the conical phase

turns the skyrmion-edge repulsion into an attraction and, consequently, there is an equilibrium distance from the edge at which the force on the skyrmions is zero. This equilibrium distance can be tuned by changing the applied magnetic field, and it acts to guide the skyrmions along the edges. We demonstrate that the specific properties of confined non-axisymmetric skyrmions offer new directions in the spintronic applications of chiral skyrmions.

The outline of this article is as follows: first, we investigate the structure of the edge states arising in the conical phase at the lateral boundaries of the system (Fig. 2). We do not include isolated skyrmions at this stage. Then, we proceed with a brief theoretical overview of isolated skyrmions within the conical phase without any influence of the edge states (Fig. 3). Based on this, we finally consider edge-skyrmion attraction in Fig. 4.

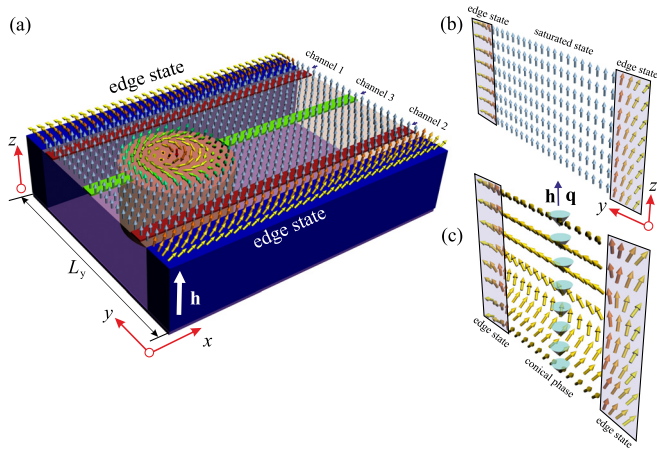
The equilibrium solutions for skyrmions and edge modulations are derived within the standard discrete model of a chiral ferromagnet where the total energy is given by

$$w = J \sum_{\langle i,j \rangle} (\mathbf{S}_i \cdot \mathbf{S}_j) - \sum_i \mathbf{H} \cdot \mathbf{S}_i - D \sum_i (\mathbf{S}_i \times \mathbf{S}_{i+\hat{x}} \cdot \hat{x} + \mathbf{S}_i \times \mathbf{S}_{i+\hat{y}} \cdot \hat{y} + \mathbf{S}_i \times \mathbf{S}_{i+\hat{z}} \cdot \hat{z}), \quad (1)$$

\mathbf{S}_i is the unit vector in the direction of the magnetization at the site i of a three-dimensional cubic lattice and $\langle i,j \rangle$ denote the pairs of nearest-neighbor spins. The first term describes the ferromagnetic nearest-neighbor exchange with $J < 0$, the second term is the Zeeman interaction, and the third term stands for the Dzyaloshinskii-Moriya (DM) interaction. The DM constant $D = J \tan(2\pi/p)$ defines the period of modulated structures p . It was established by direct calculations that in chiral ferromagnets the DM interactions strongly suppress demagnetization effects.^{2,5} In many practical cases, the surface and internal stray-field magnetostatic energy of skyrmions can be reduced to local energy contributions and included into effective magnetic anisotropy energy.^{2,5}

In what follows, we use $J = 1$ and the DM constant is set to 0.445 that corresponds to $p = 15$. We consider periodic

^{a)}A.Leonov@ifw-dresden.de



boundary conditions in z and x directions, whereas along y the stripe is confined by vertical surfaces with the free boundary conditions (Fig. 1). The size of our numerical grid is set to $2p \times 50 \times p$. In an infinite sample, below the critical field $H_D = D^2/2J$, the global minimum of (1) corresponds to the modulation phase with the propagation direction along the applied field, the *cone* phase¹⁹ (Fig. 1(c))

$$\theta_c = \arccos(H/H_D), \quad \psi_c = 2\pi z/p, \quad (2)$$

where θ, ψ are the polar and azimuthal angles of the magnetization vector.

The saturated state with $\theta = 0$ occurs when $H > H_D$. In the saturated state, isolated skyrmions are axisymmetric and translationally invariant along z .^{1,2} Chiral surface twists for $H > H_D$ have been investigated in a number of earlier contributions.^{14–16} Below H_D , the incompatibility with the longitudinally modulated conical phase imposes a complex, three-dimensional character on the magnetic modulations of the skyrmions and edge states (Figs. 2 and 3).

The solutions for edge states in the sample with the conical phase (2) in its bulk are shown in Fig. 2. The dependence $S_z(y)$ for a fixed value of x and z (Fig. 2(a)) shows the formation of two humps in the vicinity of two free surfaces xz with $y = 0$ and $y = L_y$. The S_z -component in these humps is larger than that for the cone in the middle of the sample, and for some cross-sections ($z = 5, 12$) it even goes through the state co-aligned with the field, $S_z = 1$ (shaded regions in Fig. 2(a) and the color plots in Fig. 2(b)). As the edge states are incompatible with the conical phase, they are surrounded by a strip-like “shell”—a transitional region running parallel to the boundary. The shell has the higher energy density as

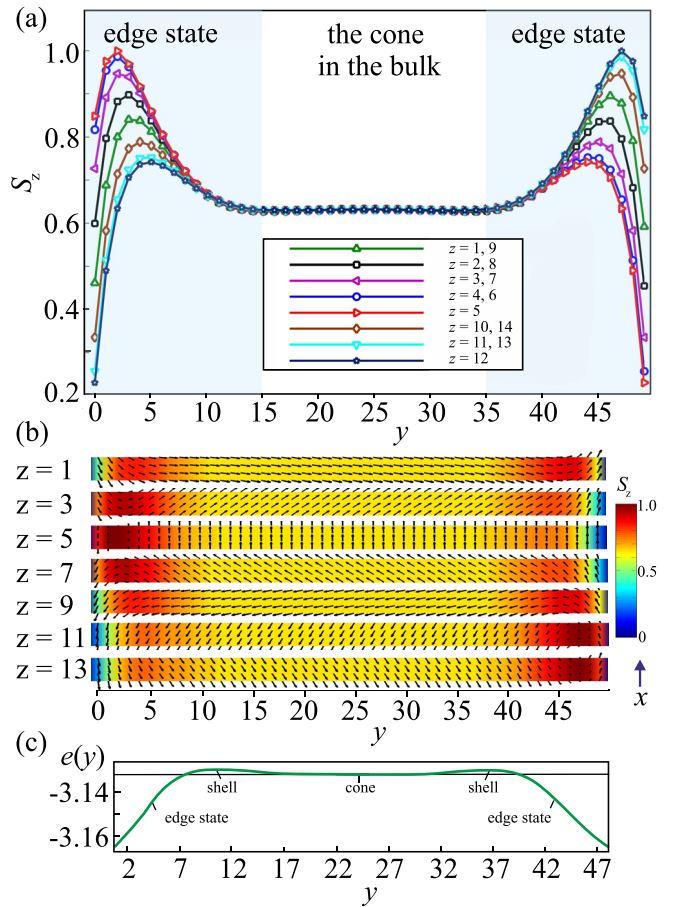


FIG. 2. Edge states in a film of a chiral magnet with the conical phase (2). (a) Variations of the magnetization component S_z along the y coordinate for fixed values of z . The blue shading indicates the regions occupied by the edge states. (b) Color plots of $S_z(x; y)$ in an xy plane with fixed values of ψ_c and z . The black arrows show in-plane spin-components. (c) The energy density $e(y)$ averaged over z (green solid line). The black thin line shows the energy density in the conical phase. The energy density is divided into constituent parts: the energy distribution near the edges, in the conical phase and in the shell which is formed due to the incompatibility of the spin structures at the edges and the conical phase in the middle of the sample.

compared with the conical phase (Fig. 2(c)) and positive exponentially decaying asymptotics.

Fig. 3 shows color plots of the energy density $w(x; y; z = \text{const})$ and skyrmion energy densities averaged over the z -coordinate, $e(\rho) = (1/p) \int_0^p w dz$, and plotted along the radial directions for isolated skyrmions within the conical phase ($H/H_D = 0.6$, Fig. 3(a)) and within the saturated state ($H/H_D = 1.1$, Fig. 3(b)). For $H > H_D$, a characteristic radius R_1 specifies the size of the skyrmionic core. The core ($\rho < R_1$) with the positive energy density is surrounded by the ring ($\rho > R_1$) with the negative energy density, which is known to form due to the DM interaction and protects isolated skyrmions from collapse.¹ The ring has the radial symmetry in all layers with the fixed z -coordinate (the color plot of $w(x; y; z = \text{const})$ in Fig. 3(b)). For $H < H_D$, $e(\rho)$ has two characteristic radii R_1 and R_2 . The skyrmionic shell is the part of the non-axisymmetric skyrmion with $\rho > R_2$ and represents an outer ring¹⁸ with the positive energy density. The color plot in Fig. 3(a) also shows that the ring with the negative energy density is partially weakened. This occurs along the radial directions where the magnetization rotates from the

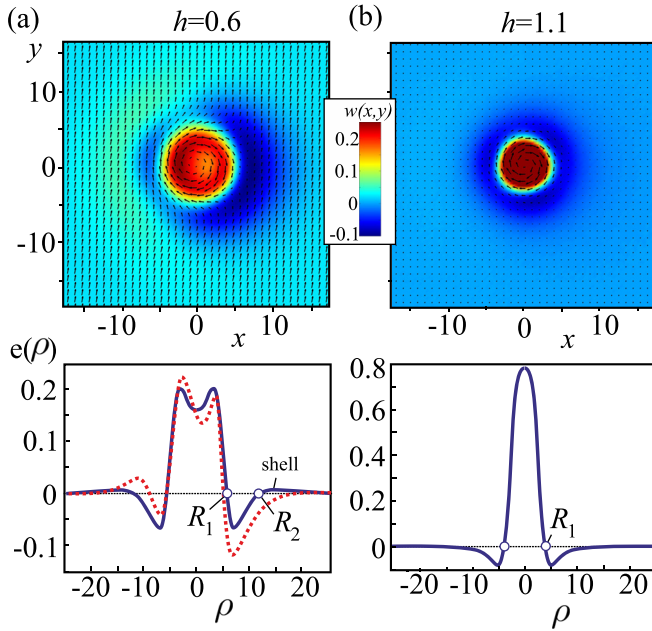


FIG. 3. Numerical solutions for isolated skyrmions obtained within the continuum version of the model (1). In (a) and (b), the isolated skyrmions are placed within different backgrounds—within the conical phase for $H/H_D = 0.6$ and the saturated state for $H/H_D = 1.1$, respectively. The first horizontal row shows two color plots of the energy density distributions $w(x, y; z = \text{const})$. The energy density is measured in units A/D^2 , where A and D are the constants of the exchange (A (grad \mathbf{m})²) and DM ($D \mathbf{m} \cdot \text{rot } \mathbf{m}$) interactions in the continuum version of (1). In the second row, the energy density $e(\rho)$ is averaged over the z -coordinate and plotted across the skyrmionic centers. The red dotted line shows the cross-section of the color plot $w(x, y; z = \text{const})$. The characteristic radius R_2 signifies the formation of a skyrmionic shell with a positive energy over the conical phase (see also [supplementary material](#)).

state opposite to the field in the center (polar angle of the magnetization $\theta = \pi$) directly to θ_c . On the contrary, the ring is restored in those parts where the magnetization rotation goes to θ_c via the state with $\theta = 0$. The attraction between skyrmions and the edges of the track occurs because the total energy can be reduced if their respective shells overlap. The skyrmion-edge interaction potentials as a function of a distance r between the skyrmion center and the ($y = 0$)-edge of the sample for different values of the applied magnetic field are plotted in Fig. 4. Potential profiles show that the attractive skyrmion-edge coupling is characterized by a rather deep potential well establishing the equilibrium separation of skyrmions from the edges. The distance $r_{\min} = \min(r)$ increases rapidly with the field. And already for $H/H_D = 0.9$, skyrmions are “released” by the edge states and are pushed to the center of the sample.

Our results open completely new perspectives on using skyrmions in nanoelectronic devices with the conical phase. First of all, the edge states with the complex spin structure give rise to a formation of two edge “channels” (schematically shown by red strips in Fig. 1), which run along the boundaries of chiral magnets and guide the skyrmions. These channels correspond to the minima of skyrmion-edge interaction potentials (Fig. 4). The distance of channels from boundaries effectively depends on the value of the applied magnetic field: for $H/H_D = 0.8$ (red line with triangular markers in Fig. 4), the channels are located farther from the boundaries and closer to each other than for $H/H_D = 0.7$ (blue line with circular

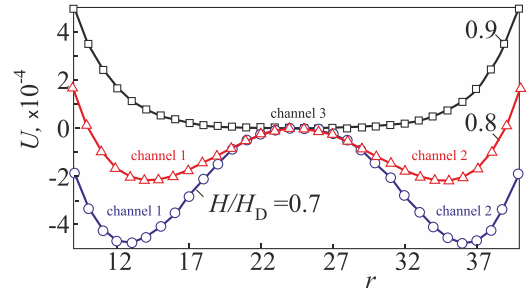


FIG. 4. The skyrmion-edge potential energy U vs. the distance r between the skyrmion center and the edge of the sample. The potential energy is measured with respect to the energy of a system for $r = L_y/2$, which corresponds to a skyrmion in the middle of the sample. $U(r)$ was calculated by imposing the constraint, $S_z = -1$, at the skyrmion center and minimizing the energy with respect to spins at all other sites. The local minima of $U(r)$ give rise to a sequence of edge channels: channels numbered 1 and 2 are located at the boundaries of the sample for $H < H_D$, and the channel 3 runs along the sample center for $H > H_D$. These channels, separated by the potential barriers, guide the motion of skyrmions.

markers in Fig. 4). For some threshold field H_{tr} , two channels numbered 1 and 2 in Figs. 1 and 4 merge into one channel 3 along the middle of the sample. The threshold field of this phenomenon depends mainly on the confinement ratio ν – the ratio of p to the width of the racetrack L_y . Due to the field-dependent position of channels, channels 1 and 2 may overlap and form channel 3 for the fields lower than H_D in narrow films. In particular, the sample used in the numerical simulations ($\nu = L_y/p = 49/15 = 3.27$) exhibits one central channel already for $H/H_D = 0.9$ in spite of the stable conical phase. H_{tr} gradually increases for wider films and reaches H_D for infinitely wide samples.

We also note that for samples confined by parallel surfaces along z -axis with $z = 0; L_z$, chiral surface twists additionally modify the structure of skyrmions near the surfaces.²⁰ These surface twists distort the translational invariance of skyrmions even in the saturated state and become evident in an additional twist of the azimuthal angle of the magnetization in skyrmions. We argue, however, that this fact does not change the attractive nature of the skyrmion-edge potential and subsequent effects.

The channel management by the applied magnetic field opens new ways to do logical operations with skyrmions on racetracks, as the information can be encoded in the lateral positions of skyrmions. Skyrmions, which fit perfectly into the edge channels, can be directed by currents along two lateral boundaries of a film and may be switched between channels by current pulses. As the potential barrier between two lateral channels is lower for larger values of the field, the lower current densities are needed to switch skyrmions between two channels. On the contrary, to ensure that the skyrmions do not jump from one channel to another due to the skyrmion Hall effect, the magnetic field must be decreased leading to the higher potential barrier between channels. Moreover, the consecutive order of skyrmions is also influenced by the value of the field, as isolated skyrmions within the conical phase attract each other and form clusters with the field-dependent inter-skyrmion distance (see for details Ref. 18). This may help to avoid clogging of skyrmionic bits as encountered in Ref. 17.

To summarize, our data have clearly demonstrated that the skyrmion-edge attraction develops in the presence of the longitudinally modulated phases and may play an important role in skyrmion-based spintronic devices (e.g., a racetrack memory design). In particular, it can be employed for magnetic patterning of nanodevices. The mechanism of skyrmion-edge attraction stems from the complex spin structures of the edge states formed at the boundaries of confined helimagnets for $H < H_D$ and isolated skyrmions embraced by the conical phase. Our results are not only relevant to the application of magnetic skyrmions in memory technology but also elucidate the fundamental properties of skyrmions and the edge states formed in the conical phases of chiral magnets.

See [supplementary material](#) for a structure evolution of an isolated non-axisymmetric skyrmion along the propagation direction of the conical phase. Color plots show $S_z(x; y)$ -components in xy planes for the varying value of z -coordinate. The color scheme is the same as in Fig. 2(b). The black arrows show the in-plane spin-components. $h = H/H_D = 0.6$, $D = 0.7265$.

The authors are grateful to M. Mostovoy and T. Monchesky for useful discussions. A.O.L acknowledges the financial support by the FOM Grant No. 11PR2928. A.N.B acknowledges the support by the Deutsche Forschungsgemeinschaft via Grant No. BO 4160/1-1.

¹A. O. Leonov, T. L. Monchesky, N. Romming, A. Kubetzka, A. N. Bogdanov, and R. Wiesendanger, *New J. Phys.* **18**, 065003 (2016).

²A. Bogdanov and A. Hubert, *J. Magn. Magn. Mater.* **138**, 255 (1994).

³N. Romming, C. Hanneken, M. Menzel, J. E. Bickel, B. Wolter, K. von Bergmann, A. Kubetzka, and R. Wiesendanger, *Science* **341**, 636 (2013);

N. Romming, A. Kubetzka, C. Hanneken, K. von Bergmann, and R. Wiesendanger, *Phys. Rev. Lett.* **114**, 177203 (2015).

⁴J. Iwasaki, M. Mochizuki, and N. Nagaosa, *Nat. Nanotechnol.* **8**, 742 (2013).

⁵N. S. Kiselev, A. N. Bogdanov, R. Schaefer, and U. K. Roessler, *J. Phys. D: Appl. Phys.* **44**, 392001 (2011).

⁶A. Fert, V. Cros, and J. Sampaio, *Nat. Nanotechnol.* **8**, 152 (2013).

⁷E. M. R. Tomasello, R. Zivieri, L. Torres, M. Carpentieri, and G. Finocchio, *Sci. Rep.* **4**, 6784 (2014).

⁸C. Moreau-Luchaire, C. Moutafis, N. Reyren, J. Sampaio, C. A. F. Vaz, N. Van Horne, K. Bouzehouane, K. Garcia, C. Deranlot, P. Warnicke, P. Wohlhüter, J.-M. George, M. Weigand, J. Raabe, V. Cros, and A. Fert, *Nat. Nanotechnol.* **11**, 444 (2016).

⁹S. Woo, K. Litzius, B. Kruger, M. Y. Im, L. Caretta, K. Richter, M. Mann, A. Krone, R. M. Reeve, M. Weigand, P. Agraval, I. Lemesch, M. A. Miawass, P. Fisher, M. Klau, and G. R. S. D. Beach, *Nat. Mater.* **15**, 501 (2016).

¹⁰X. Z. Yu, N. Kanazawa, W. Z. Zhang, T. Nagai, T. Hara, K. Kimoto, Y. Matsui, Y. Onose, and Y. Tokura, *Nat. Commun.* **3**, 988 (2012).

¹¹C. Hanneken, A. Kubetzka, K. von Bergmann, and R. Wiesendanger, *New J. Phys.* **18**, 055009 (2016).

¹²H. F. Du, R. C. Che, L. Y. Kong, X. B. Zhao, C. M. Jin, C. Wang, J. Y. Yang, W. Ning, R. W. Li, C. Q. Jin, X. H. Chen, J. D. Zang, Y. H. Zhang, and M. L. Tian, *Nat. Commun.* **6**, 8504 (2015); H. F. Du, J. P. DeGrave, F. Xue, D. Liang, W. Ning, J. Y. Yang, M. L. Tian, Y. H. Zhang, and S. Jin, *Nano Lett.* **14**, 2026 (2014).

¹³For an overview of this phenomenon and bibliography see Ref. 14.

¹⁴S. A. Meynell, M. N. Wilson, H. Fritzsche, A. N. Bogdanov, and T. L. Monchesky, *Phys. Rev. B* **90**, 014406 (2014).

¹⁵M. N. Wilson, E. A. Karhu, D. P. Lake, A. S. Quigley, S. Meynell, A. N. Bogdanov, H. Fritzsche, U. K. Röbler, and T. L. Monchesky, *Phys. Rev. B* **88**, 214420 (2013).

¹⁶R. Keesman, A. O. Leonov, S. Buhandt, G. T. Barkema, L. Fritz, and R. A. Duine, *Phys. Rev. B* **92**, 134405 (2015).

¹⁷X. C. Zhang, G. P. Zhao, H. Fangohr, J. P. Liu, W. X. Xia, J. Xia, and F. J. Morvan, *Sci. Rep.* **5**, 7643 (2015).

¹⁸A. O. Leonov, T. L. Monchesky, J. C. Loudon, and A. N. Bogdanov, *J. Phys.: Condens. Matter* **28**, 35LT01 (2016).

¹⁹P. Bak and M. H. Jensen, *J. Phys. C: Solid State Phys.* **13**, L881 (1980).

²⁰A. O. Leonov, Y. Togawa, T. L. Monchesky, A. N. Bogdanov, J. Kishine, Y. Kousaka, M. Miyagawa, T. Koyama, J. Akimitsu, Ts. Koyama, K. Harada, S. Mori, D. McGrouther, R. Lamb, M. Krajnak, S. McVitie, R. L. Stamps, and K. Inoue, *Phys. Rev. Lett.* **117**, 087202 (2016).